Available online at www.sciencedirect.com
ScienceDirect
Ceramics International 37 (2011) 231–239
CERAMICS INTERNATIONAL
www.elsevier.com/locate/ceramint

Composite cathodes of $La_{0.9}Ca_{0.1}Ni_{0.5}Co_{0.5}O_3$–$Ce_{0.8}Sm_{0.2}O_{1.9}$ for solid oxide fuel cells

Yen-Pei Fu *, Feng-Yi Tsai

Department of Material Science and Engineering, National Dong Hwa University, Shou-Feng, Hualien, 97401 Taiwan

Received 25 March 2010; received in revised form 15 July 2010; accepted 24 August 2010
Available online 29 September 2010

Abstract

The mixed ionic and electronic conductors of $La_{0.9}Ca_{0.1}Ni_{0.5}Co_{0.5}O_3$–$Ce_{0.8}Sm_{0.2}O_{1.9}$ (LCNC–SDC) are investigated systematically for potential application as a cathode for solid oxide fuel cells based on a $Ce_{0.8}Sm_{0.2}O_{1.9}$ (SDC) electrolyte. The electrochemical impedance spectroscopy (EIS) measurements are performed in air over the temperature range of 600–850 °C to determine the cathode polarization resistance. The exchange current densities for oxygen reduction reaction (ORR), determined from the low-field cyclic voltammetry, high-field cyclic voltammetry, and EIS data are systematically investigated. The activation energies (E_a) for ORR determined from the slope of Arrhenius plots are in the range of 102.33–150.73 kJ mol^{-1} for LCNC–SDC composite cathodes. The experimental results found that LCNC–SDC (70:30) composite cathode has a maximum exchange current density and a minimum polarization resistance of 0.30 Ω cm^2 for 850 °C among LCNC–SDC composite cathodes.

Keywords: A. Powders: solid state reaction; C. Electrical conductivity; E. Fuel cells

1. Introduction

Solid oxide fuel cells (SOFCs) offer an environmentally friendly alternative to heat engines in electric power because of their high energy conversion efficiency and low emission of air pollution [1–3]. Generally, yttria-stabilized zirconia (YSZ) is widely used as the electrolyte and strontium-doped lanthanum manganite (LSM) as the cathode is well-known. However, YSZ electrolyte exhibits purely ionic conductivity at high temperature (~1000 °C), such a high temperature will bring several serious problems. Example for an interfacial reaction between the electrode and electrolyte results in insulating phases, e.g., the intermediate phase of $La_2Zr_2O_7$ phase is formed at the interface between the $LaNi_zFe_{1-x}O_3$ (LNF) cathode material and zirconia electrolyte when the sintering temperature is higher than 1300 °C [4]. The formation of the $La_2Zr_2O_7$ leads to cathode degradation because the electronic and ionic conductivity of $La_2Zr_2O_7$ is very low [5].

To overcome above-mentioned drawbacks, it is important to find high performance materials for electrolyte and cathode, which can operate at intermediate-temperature (600–800 °C) SOFC. Among electrolyte materials, samaria-doped ceria (SDC) is a promising higher ionic conductivity than YSZ at intermediate-temperature among electrolyte materials [6]. Recently, there are growing interests in developing an improved performance cathode for IT-SOFCs [7–9]. Promising candidates are normally based on the mixed oxygen ionic and electronic conducting oxides such as $La_{0.6}Sr_{0.4}Co_{0.2}Fe_{0.8}O_{3-\delta}$ (LSCF) and $Ba_{0.5}Sr_{0.5}Co_{0.8}Fe_{0.2}O_{3-\delta}$ (BSCF) [10–13]. However, some disadvantages of the BSCF may include the high thermal expansion coefficient (TEC), which is as large as 21–24 × 10^{-6} and the low electrical conductivity, which is only in the range of 40–60 S/cm [14,15]. The main problems with LSCF are its large TEC and vigorous reaction with the YSZ electrolyte above 900 °C [16]. The Co-based perovskites are good candidates for intermediate-temperature solid oxide fuel cell (IT-SOFC) because of their high conductivity and good electrochemistry properties. Hrovat et al. [17] proposed that the perovskite with nominal composition$LaNi_{0.6}Co_{0.4}O_3$ has a high electronic conductivity and its TEC is 11.9 × 10^{-6} K^{-1}. The TEC of doped CeO_2 electrolytes and cathode materials were

* Corresponding author. Tel.: +886 3 863 4209; fax: +886 3 863 4200.
E-mail address: d887503@alumni.nthu.edu.tw (Y.-P. Fu).

0272-8842/$36.00
doi:10.1016/j.ceramint.2010.09.024

very close, rendering cathode materials easily attached on electrolytes. Furthermore, Ciambelli et al. [18] reported that Ca-doped $LaFeO_3$ can obtain stable perovskite structure via the substitution of Ca for La. In consideration of stabilization in perovskite structure and TEC match for doped CeO_2 electrolyte, we developed $La_{0.9}Ca_{0.1}Ni_{0.5}Co_{0.5}O_3$ (LCNC)–$Ce_{0.8}Sm_{0.2}O_{1.9}$ (SDC) composite cathode materials and evaluated these materials for use as a possible cathode.

The activation energy for oxygen diffusion and oxygen ion conductivity in cathode materials is a very important parameter to evaluate their performance. High activation energy for oxygen diffusion resulting in oxygen ion conductivities decrease rapidly as decreased in the operation temperature, leading the high interfacial resistances [19]. Therefore, it is necessary to develop a new cathode material which has high electro-catalytic activity for oxygen reduction reaction (ORR) and high oxygen ion conductivity for oxygen transport through the cathode at low temperature. Therefore, we systematically described the electrochemistry properties of the LCNC–SDC composite cathodes on the SDC electrolyte and electrochemical reaction mechanism by electrochemical impedance spectroscopy (EIS). The exchange current density, i_0, which reflects the intrinsic oxygen reduction rate is an important parameter to investigate oxygen reduction reaction mechanism at the cathode. In this study, the exchange current density values were determined using both EIS and cyclic voltammetric (CV) data [both low-field and high-field approaches] for ORR at LCNC–SDC composite cathodes.

2. Experimental

The $La_{0.9}Ca_{0.1}Ni_{0.5}Co_{0.5}O_3$ (LCNC) cathode materials were prepared by conventional solid-state reaction. First La_2O_3, $CaCO_3$, NiO, Co_3O_4 powders (>99%) were mixed and ball-milled for 12 h using ethanol as medium. The resultant mixture was dried and calcined in air at 1000 °C for 12 h. In order to get finer powder, the calcined powder was ball milled again for 12 h. $Ce_{0.8}Sm_{0.2}O_{1.9}$ (SDC) powder was synthesized by coprecipitation using $Ce(NO_3)_3{\cdot}6H_2O$ and $Sm(NO_3)_3{\cdot}6H_2O$ as the starting materials. These starting materials with stoichiometric ratio were dissolved in distilled water and then added to a solution of ammonia. The mixture solution was adjusted to a pH value in the range of 9.5–10. The resultant precipitate was vacuum filtered, and washed three times with water and ethanol, respectively. Then, the precipitate was dried at 100 °C in an oven. The coprecipitated powder was calcined in air at 600 °C for 2 h. The SDC powder sample was pelletized with a small amount of PVA as binder with an applied unaxial pressure of 1000 kgf cm^{-2} with the dimensions of 15 mm in diameter and 1 mm in thickness. The disc samples were then finally sintered at 1500 °C for 5 h with a programmed heating rate of 5 °C min^{-1} [20]. The sintered composite cathodes were characterized by X-ray powder diffractometer (XRD; Rigaku D/MAX-2500V), which recorded with scanning rate of 4° min^{-1} and scanning range 15°–75° using a Cu Kα (λ = 1.5418 Å) radiation source. The microstructure and morphological images of the cathode and cells were observed by scanning electron microscope (SEM; Hitachi 3500 H). The compositions of the LCNC–SDC composite cathodes were analyzed by energy dispersive X-ray spectroscopy (EDS).

The composite working electrode (WE) was prepared by mixing $La_{0.9}Ca_{0.1}Ni_{0.5}Co_{0.5}O_3$ (LCNC) cathode with $Ce_{0.8}Sm_{0.2}O_{1.9}$ (SDC) electrolyte powders using ball milling. These composite cathode materials consist of LCNC:SDC (in wt.%) = 70:30, 65:35, 60:40; and hereafter are identified as 70LCNC–30SDC, 65LCNC–35SDC, and 60LCNC–40SDC, respectively. The cathode paste consists of cathode powder, solvent, binder and plasticizer. The cathode paste was applied on both sides of SDC electrolyte discs with circle pattern using screen-printing method. On one side, the cathode paste was painted as the working electrode (WE) with surface area of 0.385 cm^2. The Ag reference electrode (RE) was painted with Ag paste and is away from WE about 0.3–0.4 cm. Such a distance was chosen to avoid measurement errors due to the misalignment of the working and counter electrodes [21–23]. The opposite side was counter electrode (CE) with surface area same as WE. After the cathode material was painted on electrolyte and sintered at 1000 °C for 2 h Pt gauze was used as current collector for cathode.

The testing-cell experiments were carried out over temperature ranging from 600 to 850 °C at interval of 50 °C in a furnace under air ($P_{O_2} = 0.21$ atm). Linear sweep voltammetry between −0.3 and 0.1 V with sweep rate 0.5 mV s^{-1} vs. the RE was performed by using the VoltaLab PGZ301 potentiostat. The AC impedance measurements were executed using the Solartron 1260. The frequency applied range from 100 kHz to 1 Hz at the open circuit voltage (OCV) with perturbation amplitude of 10 mV. The impedance measurements and fitting analysis were done using the Zview software. The electrolyte resistance was determined from the impedance measurements to establish the resistance free current (i)–overpotential (η) characteristics [24]. Overpotentials were calculated according to the following relation: $\eta_{WE} = \Delta U_{WR} - iR_{el}$, where η_{WE} was the applied voltage between the working electrode and the reference electrode, i was the current intensity flowing through the cell, and R_{el} was the resistance of the electrolyte measured from impedance spectrum [25,26].

3. Results and discussions

3.1. XRD and SEM of LCNC + SDC composite cathode

Fig. 1 shows the XRD pattern of the powder mixture of 50 wt.% LCNC and 50 wt.% SDC fired at 1000 °C for 2 h. The aim of this work is to investigate potential interaction between LCNC and SDC. The LCNC contains a rhombohedral perovskite structure (JCPDS powder diffraction file No. 48-0123), while SDC has a cubic fluorite-type structure (JCPDS powder diffraction file No. 75-0158), they are different phase structures. The result revealed that no obvious interface reaction appeared for the composite cathode (50 wt.% LCNC + 50 wt.% SDC) fired at 1000 °C for 2 h. A well defined perovskite LCNC oxide phase and SDC oxide phase

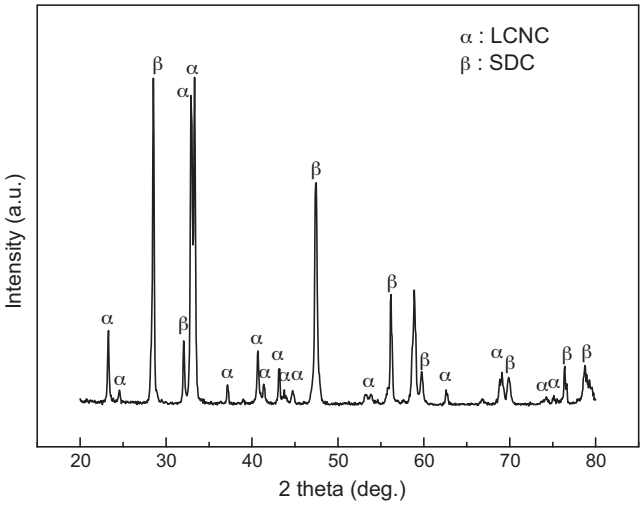

Fig. 1. X-ray diffraction pattern of the powder mixture of 50 wt.% LCNC and 50 wt.% SDC fired at 1000 °C for 2 h.

can be seen from Fig. 1. It implies that LCNC–SDC composite cathodes are chemically stable, when the firing temperature is below 1000 °C for SDC electrolyte-based SOFC.

Fig. 2a–d shows the SEM images of top-view morphology of the cathode materials of pure LCNC, 70LCNC–30SDC, 65LCNC–35SDC, and 60LCNC–40SDC, respectively. In Fig. 2a, it reveals that the grain sizes of pure LCNC cathode were uniform and distribution in the range of 1–2 μm. While in Fig. 2b–d, SDC particles formed agglomeration phenomenon, in which particle sizes are distributed in the range of 2–5 μm in composite cathode for 70LCNC–30SDC, 65LCNC–35SDC, and 60LCNC–40SDC. As shown in Fig. 3a and b, the EDS

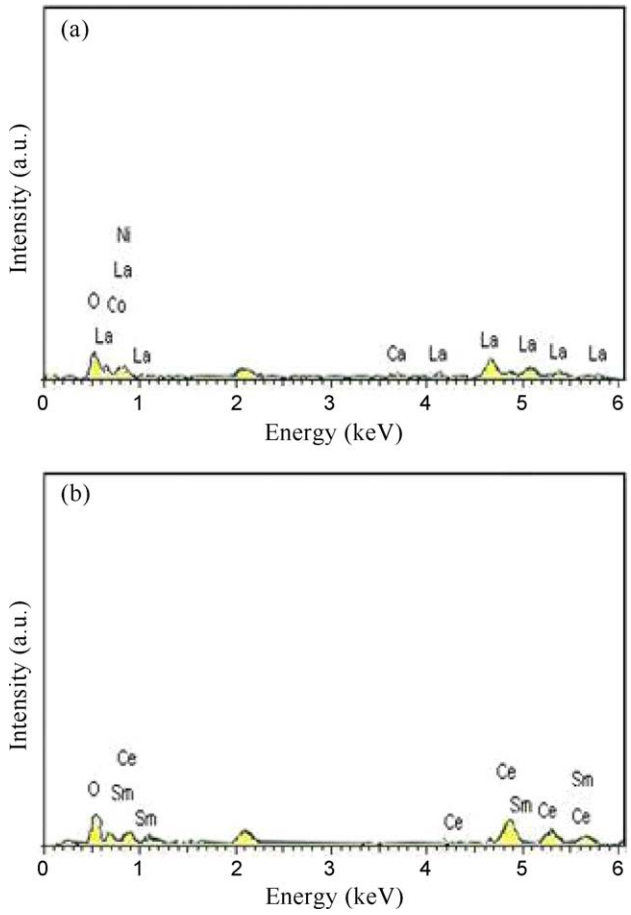

Fig. 3. EDS patterns corresponding to selected areas in b, energy unit of the horizontal axis is keV.

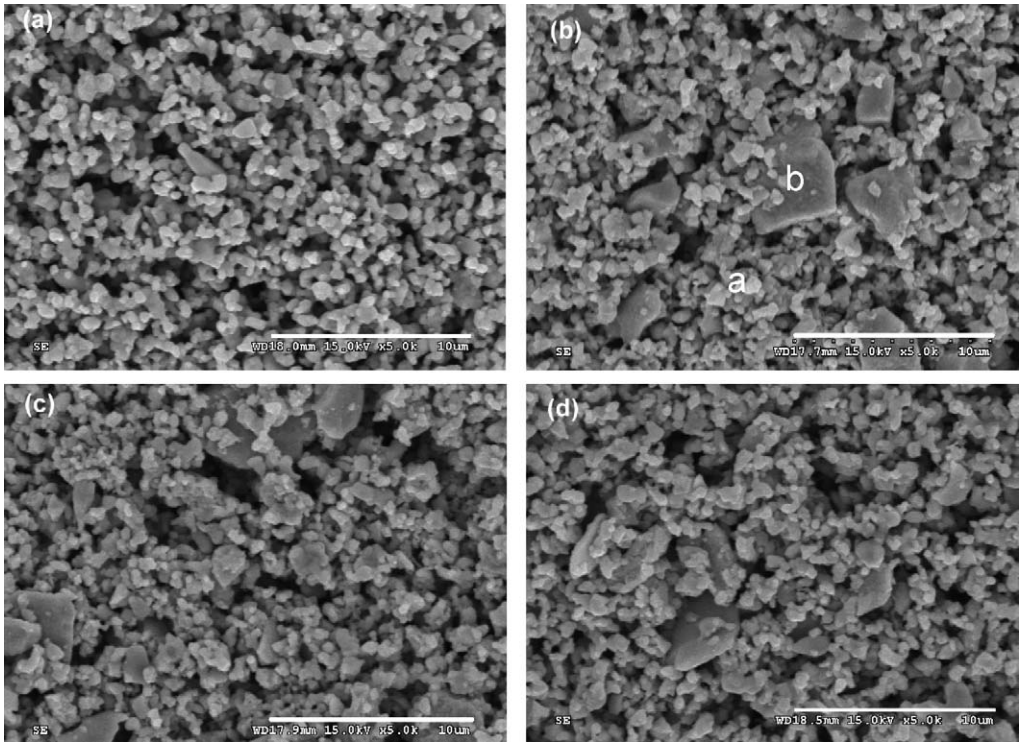

Fig. 2. SEM photograph of (a) pure LCNC, (b) 70LCNC–30SDC, (c) 65LCNC–35SDC, and (d) 60LCNC–40SDC.

Table 1
The EDS data of the 70LCNC–30SDC composite cathode for spots a and b.

Spots	Atom (%)						
	Ca K	Ce K	Co K	La K	Ni K	Sm K	O K
a	1.76	–	10.47	19.03	10.05	–	58.70
b	–	26.22	–	–	–	5.37	68.40

patterns corresponding to selected areas in Fig. 2b and their EDS data are listed in Table 1. The results show LCNC cathode with uniform and fine particle size, however SDC electrolyte with coarse and large particle size. In general, composite cathode material sintered at high temperature with larger grain size leading to the decrease in the electrode surface area-gas solid interface (triple phase boundary, TPB), which resulted in high polarization resistance [27,28]. While, due to the high sintering temperature, the cathode materials adhered strongly to the SDC electrolyte surface resulting in a better contact with the electrolyte and made sure a better current collection. It was a trade-off relationship with regard to the sintering temperature to obtain cathode materials with fine microstructure and strong adhesion to the electrolyte [28]. Fig. 4 shows the interface between pure LCNC cathode and SDC electrolyte sintered at 1000 °C, which indicates LCNC cathode sintered at 1000 °C with the grain sizes of 1–2 μm, pore sizes of 2–3 μm and good adhesion to the electrolyte. No obvious cracks appeared at the interface between LCNC cathode and SDC electrolyte. The thickness of LCNC layer was about 30 μm, the porosity, as described, is thought to be sufficient to guarantee a gas fast diffusion. Such interface with reasonable porosity and good adhesion effectively reduces the polarization resistance and enhances the current collection.

3.2. Interfacial (cathode) polarization resistances

Impedance for symmetrical LCNC–SDC/SDC/LCNC–SDC testing cells sintered at 1000 °C for 2 h, which recorded under open-circuit condition in air. The ohmic resistance was eliminated in the impedance plot to facilitate easy comparison of cathode polarization resistance. The polarization resistance of LCNC–SDC composite cathode was measured directly from the difference between high- and low-frequency intercepts on the real axis of the impedance plot [29]. Fig. 5 shows the impedance spectra measured under open-circuit condition at 800 °C in air for LCNC–SDC composite cathodes. In this study, we take middle-frequency as the core for the fitting curve. The simple equivalent circuit $R_1(R_2/\mathrm{CPE})$ of the impedance curve is used for symmetrical LCNC–SDC/SDC/LCNC–SDC testing cells as shown in Fig. 5e. A parallel RC element represents a drop capacitor with a typical relaxation time which corresponds to the process. In the present case, in place of capacitor a constant phase element (CPE) is applied to model the experimental data. The CPE is equivalent to a distribution of capacitors in parallel. R_1 represents an ohmic resistance of the cell and R_2 represents the resistance corresponding to the cathode polarization. CPE can be expressed as follows, $Z = 1/(C(j\omega)^n)$, where C indicates the ideal capacitance ($n = 1$),

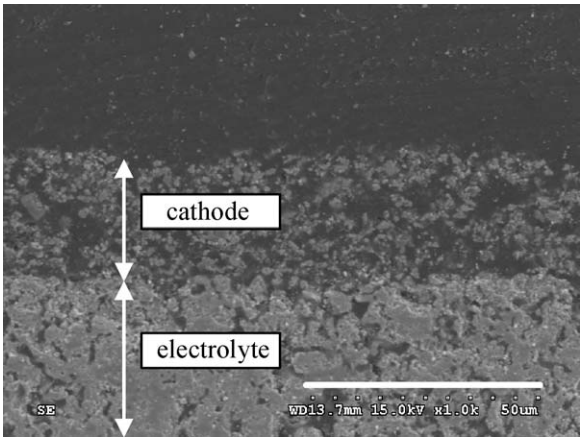

Fig. 4. SEM image (cross-section view) for the interfaces between pure LCNC cathode and SDC electrolyte sintered at 1000 °C for 2 h.

$j = (-1)^{1/2}$, and ω is the angular frequency and the values of n describes the fractal character (the heterogeneous or porous character) of the sample, where the value is between 0 and 1 [30]. Table 2 shows the values of fitting parameter of LCNC–SDC composite cathodes as a function of temperature in air. In all specimens, it can be observed that R_1 and R_2 decrease dramatically with increasing temperature. As the testing temperature increases above 800 °C, the 70LCNC–30SDC composite cathode has the lowest R_2 value indicating that the resistance corresponding to the cathode polarization is affected by not only microstructure but also composition of composite cathode.

Fig. 6 shows the temperature dependence of the Arrhenius plot of interfacial (cathode polarization) resistance for LCNC–SDC composite cathodes. From the plot, it can be seen that cathode polarization resistance decreases rapidly with the increasing temperature. The activation energy is calculated from the slopes of the Arrhenius plot of interfacial resistance vs. $1000/T$. Waller et al. [31] reported that the cathode with nano- and submicron-structure during sintering process could obtain

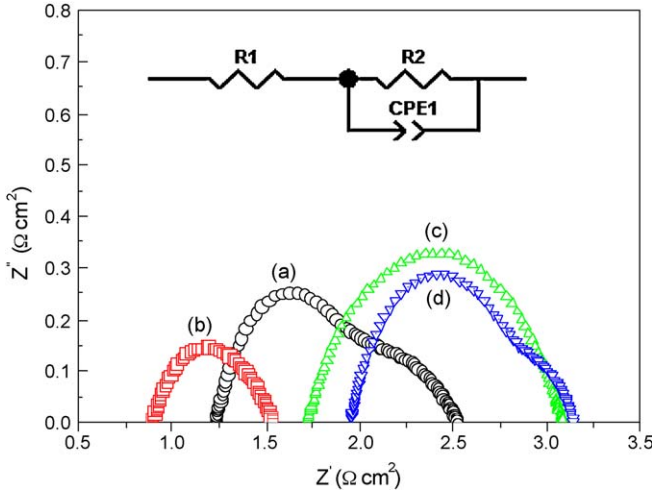

Fig. 5. Impedance spectrums for LCNC–SDC composite cathodes measured under open-circuit condition at 800 °C for (a) pure LCNC, (b) 70LCNC–30SDC, (c) 65LCNC–35SDC, (d) 60LCNC–40SDC and the equivalent circuit.

Table 2
Results of fitting parameter of LCNC–SDC composite cathodes measured at different temperatures.

Cathode	750 °C		800 °C		850 °C	
	R_1 (Ω cm^2)	R_2 (Ω cm^2)	R_1 (Ω cm^2)	R_2 (Ω cm^2)	R_1 (Ω cm^2)	R_2 (Ω cm^2)
LCNC	1.97	1.87	1.22	1.28	0.99	0.61
70LCNC–30SDC	1.01	1.17	0.88	0.63	0.58	0.30
65LCNC–35SDC	2.13	2.04	1.73	1.24	1.36	0.63
60LCNC–40SDC	3.78	3.24	1.95	1.17	1.52	0.65

low activation energy for cathode polarization resistance. This can be explained as a good adhesion exists between electrolyte and cathode. Therefore, the cathode with continuous and three dimension framework provided the gas a pathway for easier transport that could effectively reduce activation energy. The activation energy of cathode polarization resistance was ∼127.7 kJ mol^{-1} for pure LCNC cathode. The activation energy of LCNC–SDC composite cathodes was distributed in the range of 110.7–142.5 kJ mol^{-1}. These values were slightly lower than LSCF–GDC (∼158.8 kJ mol^{-1}) composite cathode reported in Ref. [22]. The activation energy of the cathode polarization resistance associated with composition of composite cathodes as well as both the medium- and low-frequency arcs.

3.3. Electrochemical of oxygen reduction reaction (ORR)

Generally speaking, the oxygen reduction can be divided into several elemental steps: (1) diffusion of oxygen molecule in the gas phase to the electrode, (2) oxygen dissociate adsorption on cathode surface, (3) surface diffusion of oxygen on the cathode, (4) incorporation of oxygen into electrolyte via the triple phase boundary (TPB), (5) oxide ion diffusion in the bulk of cathode, and oxide ion transfer from cathode to electrolyte [32,33]. The exchange current density, i_0, which reflects the intrinsic oxygen reduction rate is an important parameter to investigate oxygen reduction reaction mechanism at the cathode [34]. The i_0 value can be obtained from the AC impedance measurement (EIS). In this technique, i_0 was measured from the polarization resistance, R_p of the Nyquist plot and calculated using Eq. (1) which is derived from the Bulter–Volmer equation [35]:

$$i_0 = \frac{RT\nu}{nFR_p} \tag{1}$$

Here n is the total number of electrons passed in the reaction, ν reflects the number of times the rate-determining step occurs for one occurrence of the full reaction, F is the Faraday constant, R is the gas constant. For the ORR, n and ν are generally assumed to be 4 and 1, respectively (as the total number of electrons passed per molecule of oxygen reduced is 4 and the rate limiting step would likely have a stoichiometry of 1 for the oxygen reduction reaction) [36]. Cyclic voltammetry (CV) results for LCNC–SDC composite cathodes are shown in Fig. 7 indicating the dependence of current with respect to the applied potential at 600–850 °C in 50 °C increments. At higher temperature, CVs show a more linear response compared to those at lower temperature, as confirmed with the earlier literature report [37].

At low overpotentials, i_0 was determined using the low-field approximation of i vs. η, where i_0 can be obtained from the slope of the i vs. η plots (Fig. 7.) using the low field approximation and calculated from Eq. (2). The slopes were determined within ±30.1, 31.8, 33.5, 35.3, 37.1 and 38.7 mV for 600, 650, 700, 750, 800 and 850 °C, respectively.

$$i_0 = \frac{RT\nu}{nF}\,\text{slope} \tag{2}$$

At high field, i_0 can be obtained from the y-intercept of the i vs. η plots (Fig. 8.) using the high field approximation and calculated using Eq. (3).

$$\log i = \log i_0 + \frac{\alpha nF}{2.3RT}\eta \tag{3}$$

where η is the cathodic polarization and α, the transfer coefficient, $\alpha = \gamma/\nu + r\beta = 0.5$, where γ, r and β are, respectively, the number of electrons passed before the rate limiting step, the number of electrons passed in the rate limiting step, and the symmetry coefficient, normally assumed to be 0.5 [38].

Values for i_0 values of LCNC–SDC composite cathodes measured from Eqs. (1)–(3) for EIS, low-field, and high field, respectively are given in Tables 3–6. In all specimens, regardless of the measurement techniques including EIS, low-field, and high-field, i_0 values increase with increasing the testing cells' temperature in all specimens. In this study, the i_0

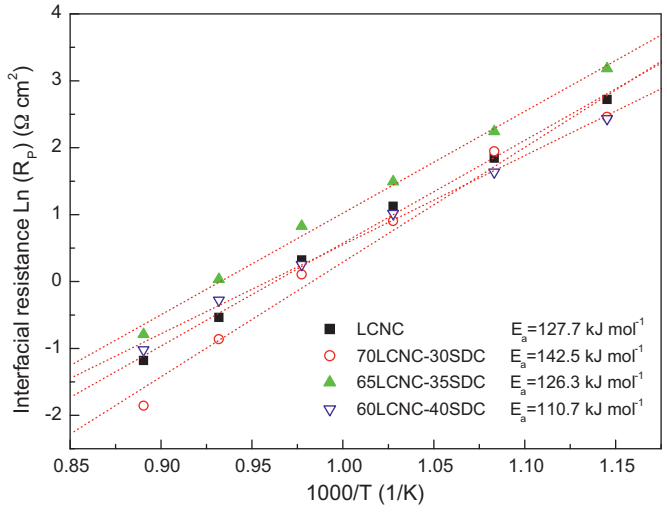

Fig. 6. Arrhenius plot of the interfacial (cathode polarization) resistances as a function of temperature for LCNC–SDC composition cathodes.

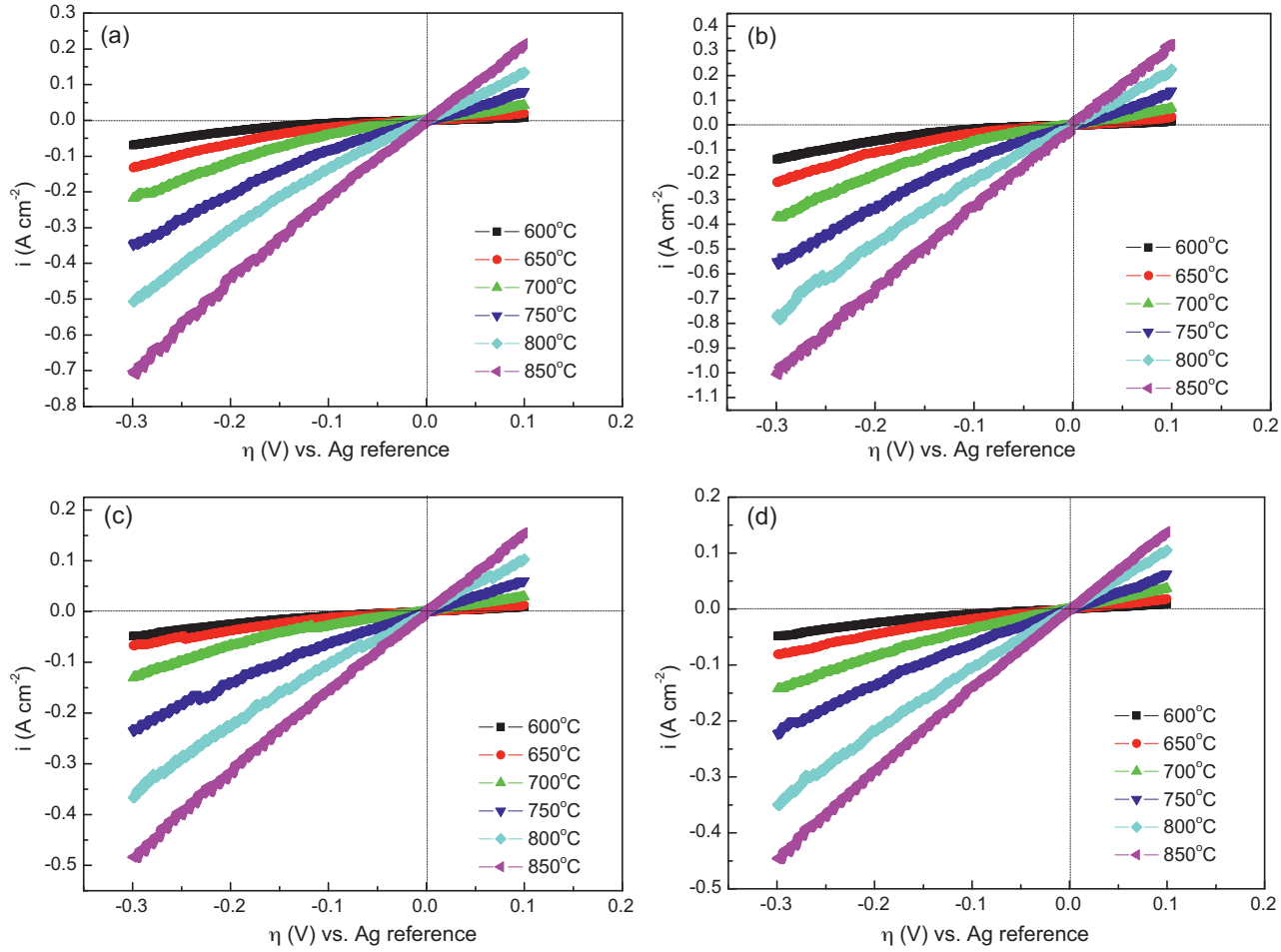

Fig. 7. The cyclic voltammograms of (a) pure LCNC, (b) 70LCNC–30SDC, (c) 65LCNC–35SDC, and (d) 60 LCNC–40SDC cathode on SDC electrolyte in air.

value determined by high-field is largest among three techniques. The i_0 values measured with various methods can be ranked as high-field > low-field > EIS. The results show a good correlation between the three techniques, revealing the validity of these measurements. The result showed that the exchange current density (i_0) of 70LCNC–30SDC composite cathode was largest compared with the other composite cathodes, demonstrating that LCNC cathode mixed with an appropriate amount of SDC electrolyte can improve the oxygen reduction reaction (ORR) activity of symmetrical LCNC–SDC/SDC/LCNC–SDC testing cells. Table 7 shows the value of exchange current density (i_0) of different cathodes. It indicates that the reasonable performance for electrocatalytic activity of 70LCNC–30SDC is achieved above the temperature of 850 °C. This suggests that 70LCNC–30SDC composite cathode may find application in conventional SOFC operating temperature.

Fig. 9 shows the Arrhenius plots for i_0 values collected at LCNC–SDC/SDC/LCNC–SDC testing cells between 600 and 850 °C, using the three techniques. From the slope of the line in the Arrhenius plots, the overall activation energy for the ORR was determined by the following equation:

$$\ln i_0 = \ln K - \frac{E_a}{RT} \quad (4)$$

Table 3
i_0 values for the ORR at LCNC cathode using low-field CV, high-field CV, and EIS measured at 600–850 °C.

T (°C)	i_0 (mA cm^{-2})		
	Low-field	High-field	EIS
600	0.95	2.02	0.63
650	2.91	5.48	1.61
700	7.21	13.31	3.47
750	16.80	28.33	8.14
800	31.10	50.86	20.17
850	55.50	81.53	40.19

Table 4
i_0 values for the ORR at 70LCNC–30SDC composite cathode using low-field CV, high-field CV, and EIS measured at 600–850 °C.

T (°C)	i_0 (mA cm^{-2})		
	Low-field	High-field	EIS
600	1.73	3.90	0.82
650	4.66	10.16	1.45
700	11.99	21.75	4.34
750	27.86	44.14	10.12
800	54.59	82.31	27.94
850	86.87	129.48	79.05

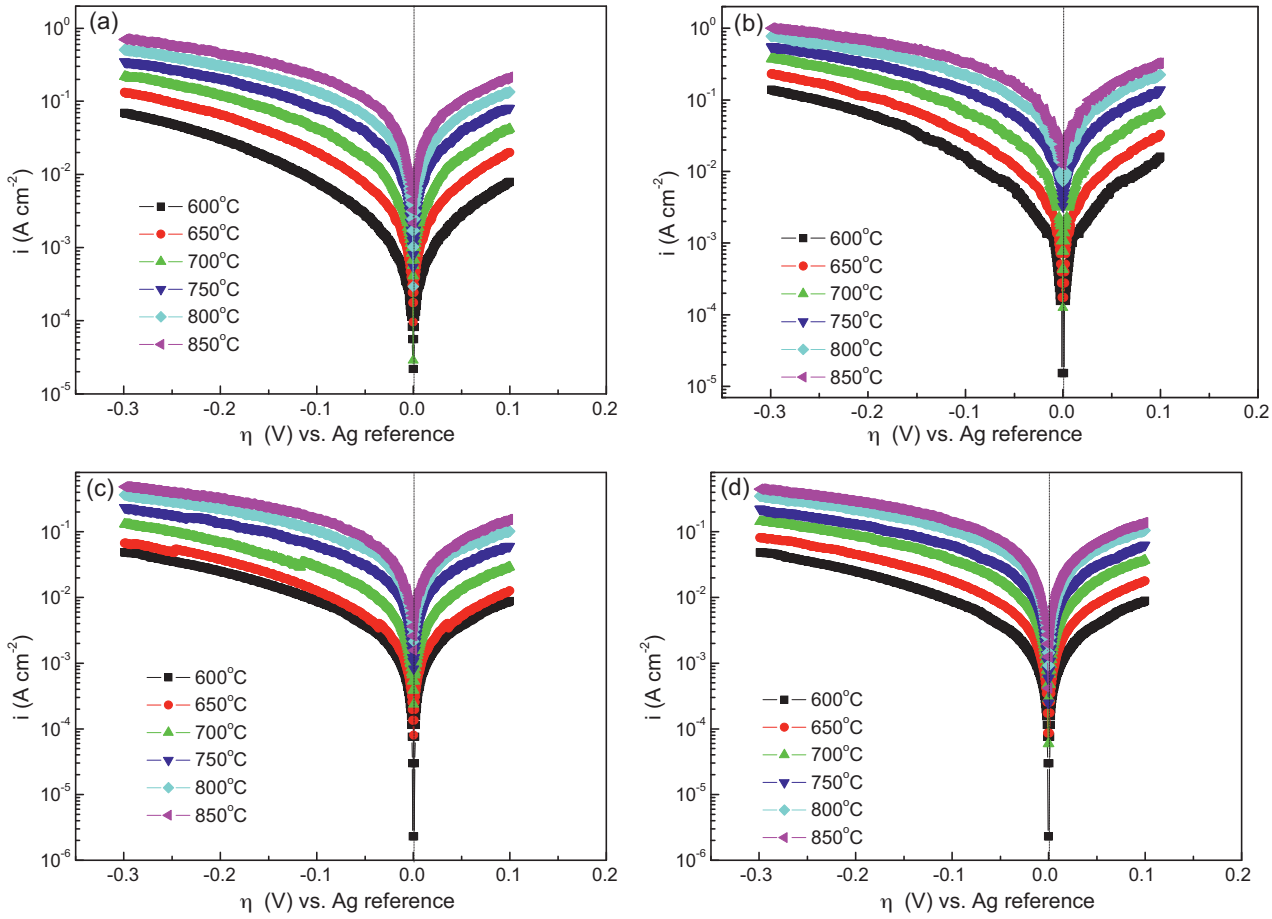

Fig. 8. Tafel plots at 0.5 mV s^{-1} between 100 mV and −300 mV of the ORR at (a) pure LCNC, (b) 70LCNC–30SDC, (c) 65LCNC–35SDC, and (d) 60LCNC–40SDC on SDC electrolyte at 600–850 °C in air.

Table 5
i_0 values for the ORR at 65LCNC–35SDC composite cathode using low-field CV, high-field CV, and EIS measured at 600–850 °C.

T (°C)	i_0 (mA cm^{-2})		
	Low-field	High-field	EIS
600	1.22	2.75	0.40
650	2.36	3.98	1.08
700	6.00	9.78	2.40
750	14.73	22.97	4.92
800	28.58	41.95	11.42
850	39.91	63.44	27.21

where K is the pre-exponential constant, which can be calculated from the y-intercept, and E_a is the reaction activation energy [37]. The activation energy (E_a) for the ORR may be related to different cathode preparation methods, the structure of cathode, or different cathode compositions. The ORR activation energy obtained from the slope of the Arrhenius plots is in the range of 102.33–150.73 kJ mol^{-1} for LCNC–SDC composite cathodes. These values are reasonable and compare well to the E_a values of 100–160 kJ mol^{-1} reported in the literatures [36,39,40]. The linearity of the Arrhenius plots in Fig. 9 indicates that LCNC–SDC composite cathodes are stable as a function of temperature.

Table 6
i_0 values for the ORR at 60LCNC–40SDC composite cathode using low-field CV, high-field CV, and EIS measured at 600–850 °C.

T (°C)	i_0 (mA cm^{-2})		
	Low-field	High-field	EIS
600	1.48	2.70	0.84
650	3.29	5.96	1.98
700	7.68	14.13	3.87
750	13.39	24.46	8.72
800	25.63	43.10	15.59
850	35.75	57.47	34.26

Table 7
Exchange current density (i_0) of the ORR for various cathodes.

T (°C)	i_0 (EIS) (mA cm^{-2})			
	70LCNC–30SDC	LSCF [26]	LSM–YSZ [26]	LSM–YSZ [27]
600	0.82	13	0.45	2.4
650	1.45			
700	4.34	65	5.8	31
750	10.12			
800	17.95			
850	79.05			

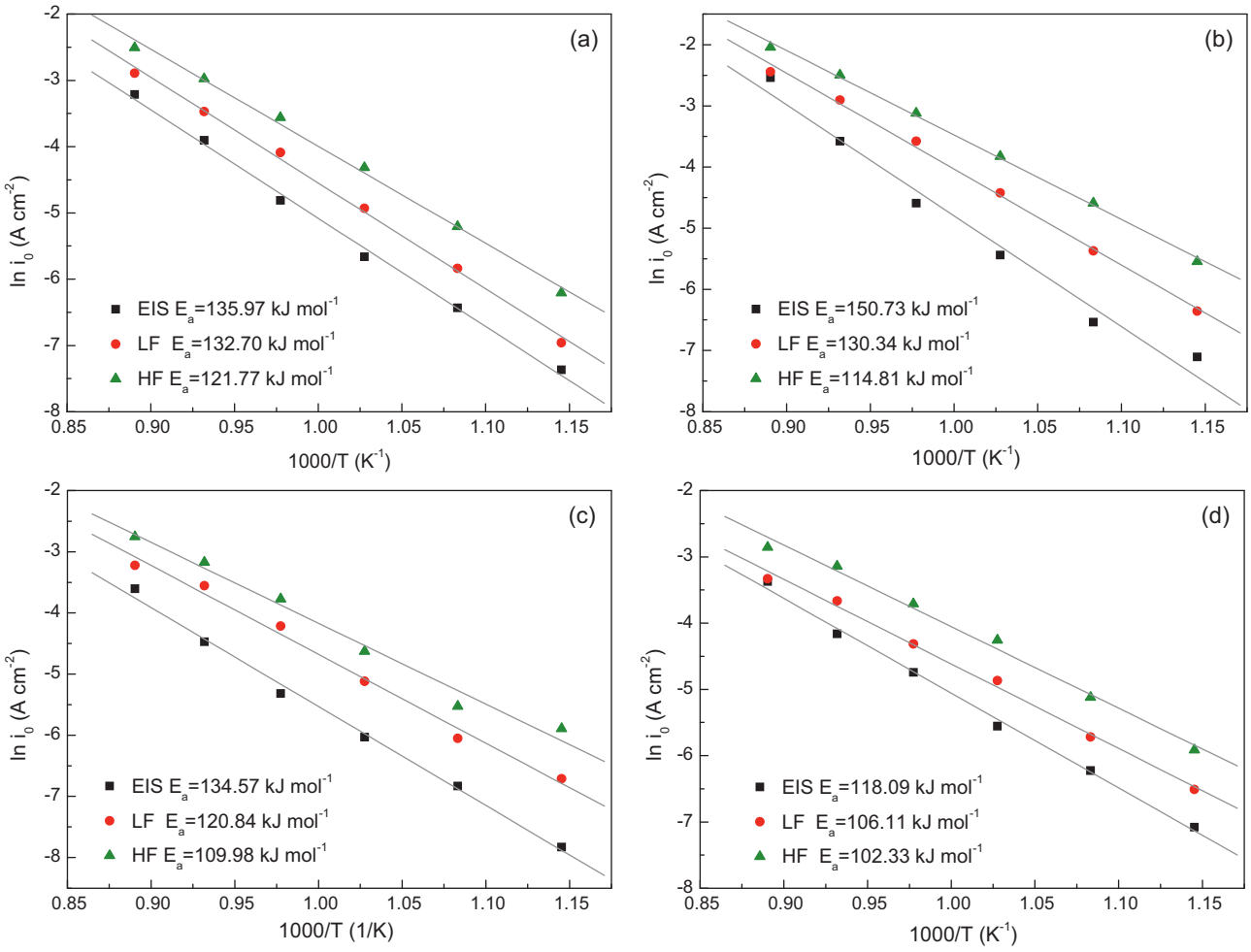

Fig. 9. Arrhenius plots for ORR at (a) pure LCNC, (b) 70LCNC–30SDC, (c) 65LCNC–35SDC, and (d) 60LCNC–40SDC in air. i_0 was obtained using the low-field, high field, and EIS technique.

4. Conclusions

In this study, $La_{0.9}Ca_{0.1}Ni_{0.5}Co_{0.5}O_3$–$Ce_{0.8}Sm_{0.2}O_{1.9}$ (LCNC–SDC) composite cathodes are reported for potential application for intermediate-temperature solid oxide fuel cells. X-ray powder diffraction examination reveals no obvious solid-state reaction between LCNC and SDC at the temperature of 1000 °C. The kinetics of oxygen reduction reaction (ORR) are investigated at LCNC–SDC composite cathodes, deposited by screen-printing on SDC electrolyte, using electrochemical impedance spectroscopy (EIS) and cyclic voltammetry (CV) at temperatures over the temperature range of 600–850 °C. The exchange current density (i_0) values are determined using both EIS and cyclic voltammetric (CV) data [both low-field and high-field approaches] for ORR. The activation energies (E_a) for ORR determined from the slope of Arrhenius plots are in the range of 102.33–150.73 kJ mol^{-1}. The experimental results found that 70LCNC–30SDC composite cathode has a high exchange current density and the minimum polarization resistance among LCNC–SDC composite cathodes suggesting a potential application as the cathode for solid oxide fuel cells.

Acknowledgements

The authors would like to thank the National Science Council of Taiwan for financially supporting this research under Contract No. NSC 98-2113-M-259-002.

References

[1] M. Mogenson, K.V. Jensen, M.J. Jorgensen, S. Primdahl, Progress in understanding SOFC electrodes, Solid State Ionics 150 (2002) 123–129.
[2] T. Hibino, A. Hashimoto, T. Inoue, J.-I. Tokuno, S.-I. Yoshida, M. Sano, A low-operating-temperature solid oxide fuel cell in hydrocarbon–air mixtures, Science 288 (2000) 2031–2033.
[3] K. Eguchi, Ceramic materials containing rare earth oxides for solid oxide fuel cell, J. Alloys Compd. 250 (1997) 486–491.
[4] J. Kundsen, P.B. Friehling, N. Bonanos, Effect of A-site stoichiometry on phase stability and electrical conductivity of the perovskite $La_s(Ni_{0.59}Fe_{0.41})O_{3-\delta}$ and its compatibility with $(La_{0.85}Sr_{0.15})_{0.91}MnO_{3-\delta}$ and $Zr_{0.85}Y_{0.15}O_{2.925}$, Solid State Ionics 176 (2005) 1563–1569.
[5] R. Chiba, Y. Tabata, T. Komatsu, H. Orui, K. Nozwa, M. Arakawa, H. Arai, Property change of a $LaNi_{0.6}Fe_{0.4}O_3$ cathode in the initial current loading process and the influence of a ceria interlayer, Solid State Ionics 178 (2008) 1701–1709.

[6] B.C.H. Steels, Appraisal of $Ce_{1-y}Gd_yO_{2-y/2}$ electrolytes for IT-SOFC operation at 500 °C, Solid State Ionics 129 (2000) 95–110.
[7] X.D. Zhu, K.N. Sun, N.Q. Zhang, X.B. Chen, L.J. Wu, D.C. Jia, Improved electrochemical performance of $SrCo_{0.8}Fe_{0.2}O_{3-\delta}$–$La_{0.45}Ce_{0.55}O_{2-\delta}$ composite cathodes for IT-SOFC, Electrochem. Commun. 9 (2007) 431–435.
[8] Z. Lei, Q. Zhu, L. Zhao, Low temperature processing of interlayer-free $La_{0.6}Sr_{0.4}Co_{0.2}Fe_{0.8}O_{3-\delta}$ cathodes for intermediate temperature solid oxide fuel cells, J. Power Sources 161 (2006) 1169–1175.
[9] S.P. Jiang, W. Wang, Fabrication and performance of GDC-impregnated (La,Sr)MnO_3 cathodes for intermediate temperature solid oxide fuel cells, J. Electrochem. Soc. 152 (2005) A1398–A1408.
[10] T. Horita, K. Yamaji, N. Sakai, H. Yokokawa, A. Weber, E. Ivers-Tiffee, Electrode reaction of $La_{1-x}Sr_xCoO_{3-\delta}$ cathodes on $La_{0.8}Sr_{0.2}Ga_{0.8}Mg_{0.2}O_{3-y}$ electrolyte in solid oxide fuel cells, J. Electrochem. Soc. 148 (5) (2001) A456–A462.
[11] C. Fu, K. Sun, N. Zhang, X. Chen, D. Zhou, Electrochemical characteristics of LSCF–SDC composite cathode for intermediate temperature SOFC, Electrochim. Acta 52 (2007) 4589–4594.
[12] Q.L. Liu, K.A. Khor, S.H. Chan, High-performance low-temperature solid oxide fuel cell with novel BSFC cathode, J. Power Sources 161 (2006) 123–128.
[13] Y. Zhang, J. Liu, X. Huang, Z. Lu, W. Su, Low temperature solid oxide fuel cell with $Ba_{0.5}Sr_{0.5}Co_{0.8}Fe_{0.2}O_3$ cathode prepared by screen printing, Solid State Ionics 179 (2008) 250–255.
[14] S. McIntosh, J.F. Vente, W.G. Haije, D.H.A. Blank, H.J.M. Bouwmeester, Oxygen stoichiometry and chemical expansion of $Ba_{0.5}Sr_{0.5}Co_{0.8}Fe_{0.2}O_{3-\delta}$ measured by in situ neutron diffraction, Chem. Mater. 18 (2006) 2186–2193.
[15] Y. Wang, S. Wang, Z. Wang, T. Wen, Z. Wen, Performance of $Ba_{0.5}Sr_{0.5}Co_{0.8}Fe_{0.2}O_{3-\delta}$-CGO-Ag cathode for IT-SOFCs, J. Alloys Compd. 428 (2007) 286–289.
[16] H.Y. Tu, Y. Takeda, N. Imanishi, O. Yamamoto, $Ln_{0.4}Sr_{0.6}Co_{0.8}Fe_{0.2}O_{3-\delta}$ (Ln = La, Pr, Nd, Sm, Gd) for the electrode in solid oxide fuel cells, Solid State Ionics 117 (1999) 277–281.
[17] M. Hrovat, N. Katsarakis, K. Reichmann, S. Bernik, D. Kuscer, J. Holc, Characterisation of $LaNi_{1-x}Co_xO_3$ as a possible SOFC cathode material, Solid States Ionics 83 (1996) 99–105.
[18] P. Ciambelli, S. Cimino, L. Lisi, M. Faticanti, G. Minelli, I. Pettiti, P. Porta, La, Ca and Fe oxide perovskites: preparation, characterization and catalytic properties for methane combustion, Appl. Catal. B 33 (2001) 193–203.
[19] J. Drennan, C.P. Travares, B.C.H. Steels, An electron microscope investigation of phases in the system La–Ni–O, Mater. Res. Bull. 17 (1982) 621–626.
[20] Y.P. Fu, S.B. Wen, C.H. Lu, Preparation and characterization of samaria-doped ceria electrolyte materials for solid oxide fuel cells, J. Am. Ceram. Soc. 91 (2008) 127–131.
[21] S.B. Adler, B.T. Henderson, M.A. Wilson, D.M. Taylor, R.E. Richards, Reference electrode placement and seals in electrochemical oxygen generators, Solid State Ionics 134 (2000) 35–42.
[22] J. Winkler, P.V. Hendriksen, N. Bonanos, M. Mogensen, Geometric requirements of solid electrolyte cells with a reference electrode, J. Electrochem. Soc. 145 (1998) 1184–1192.
[23] S.H. Chan, X.J. Chen, K.A. Khor, Reliability and accuracy if measured overpotential in a three-electrode fuel cell system, J. Appl. Electrochem. 31 (2001) 1163–1170.
[24] Z. Gao, Z. Mao, J. Huang, R. Gao, C. Wang, Z. Liu, Composite cathode $La_{0.15}Bi_{0.85}O_{1.5}$–Ag for intermediate-temperature solid oxide fuel cells, Mater. Chem. Phys. 108 (2008) 290–295.
[25] F. Mauvy, C. Lalanne, J.M. Bassat, J.C. Grenier, H. Zhao, P. Dordor, P. Stevens, Oxygen reduction on porous $Ln_2NiO_{4+\delta}$ electrodes, J. Eur. Ceram. Soc. 25 (2005) 2669–2672.
[26] C.R. Xia, W. Rauch, F.L. Chen, M.L. Liu, $Sm_{0.5}Sr_{0.5}CoO_3$ cathodes for low-temperature SOFCs, Solid State Ionics 149 (2002) 11–19.
[27] H.J. Hwang, J.W. Moon, J. Moon, Removal of nitric oxide (NO) by perovskite-type composite catalytic thick film, $La_{0.6}Sr_{0.4}Co_{0.2}Fe_{0.8}O_{3-\delta}$ and gadolinia-doped ceria electrolyte, $Gd_{0.2}Ce_{0.8}O_2$, J. Am. Ceram. Soc. 88 (2005) 79–84.
[28] H.J. Hwang, M.J. Woong, L. Seunghun, E.A. Lee, Electrochemical performance of LSCF-based composite cathodes for intermediate temperature SOFCs, J. Power Sources 145 (2005) 243–248.
[29] Y. Leng, S.H. Chan, Q. Liu, Development of LSCF–GDC composite cathodes for low-temperature solid oxide fuel cells with thin film GDC electrolyte, Int. J. Hydrogen Energy 33 (2008) 3808–3817.
[30] J.X. Zhu, D.F. Zhou, S.R. Guo, J.F. Ye, X.F. Hao, X.Q. Cao, J. Meng, Grain boundary conductivity of high purity neodymium-doped ceria nanosystem with and without the doping of molybdenum oxide, J. Power Sources 174 (2007) 114–123.
[31] D. Waller, J.A. Lane, J.A. Kilner, B.C.H. Steele, The effect of thermal treatment on the resistance of LSCF electrodes on gadolinia doped ceria electrolytes, Solid State Ionics 86–88 (1996) 767–772.
[32] M. Kleitz, F. Petitbon, Optimized, SOFC, Electrode microstructure, Solid States Ionics 92 (1996) 65–74.
[33] A. Ringuede, J. Fouletier, Oxygen reaction on strontium-doped lanthanum cobaltite dense electrodes at intermediate temperatures, Solid States Ionics 139 (2001) 167–177.
[34] S.B. Adler, Factors governing oxygen reduction in solid oxide fuel cell cathodes, Chem. Rev. 104 (2004) 4791–4844.
[35] J. Piao, K. Sun, N. Zhang, X. Chen, S. Xu, D. Zhou, Preparation and characterization of $Pr_{1-x}Sr_xFeO_3$ cathode material for intermediate temperature solid oxide fuel cells, J. Power Sources 172 (2007) 633–640.
[36] J. Liu, A.C. Co, S. Paulson, V.I. Birss, Oxygen reduction at sol–gel derived $La_{0.8}Sr_{0.2}Co_{0.8}Fe_{0.2}O_3$ cathodes, Solid State Ionics 177 (2006) 377–387.
[37] A.C. Co, S.J. Xia, V.I. Briss, A kinetic study of the oxygen reduction reaction at $LaSrMnO_3$–YSZ composite electrodes, J. Electrochem. Soc. 152 (2005) A570–A576.
[38] J.O.M. Bockris, A.K.N. Reddy, Modern Electrochemistry: An Introduction to an Interdisciplinary Area, Plenum Publishing Corporation, New York, 1977.
[39] R. Doshi, V.L. Richards, J.D. Carter, X. Wang, M. Krumpelt, Development of solid-oxide fuel cells that operate at 500 °C, J. Electrochem. Soc. 146 (1999) 1273–1278.
[40] K. Sasaki, J. Tamura, H. Hosoda, T.N. Lan, K. Yasumoto, M. Dokiya, Pt–perovskite cermet cathode for reduced-temperature SOFCs, Solid State Ionics 148 (2002) 551–555.